Chapter 3

Topological entanglement entropy to identify topological order in quantum skyrmions

3.1 Introduction

Distinct values of a quantity referred to as the topological invariant characterise topological phases. This quantity stays constant under smooth deformations (which do not close the bulk energy gap) when the system is in a topological phase [168]. This property of a topological phase can be referred to as topological protection. In other words, we can not move from one topological phase to another without encountering a phase transition.

In this work, we are interested in one of the highly promising topological entities called skyrmions. They have peculiar non-collinear spin textures [116, 117, 118, 169, 170, 171]. Despite the small size, nontrivial topological characteristics confer them with a remarkable degree of thermal stability even at room temperature [172, 173, 174, 175, 176, 177, 178]. Owing to these properties, skyrmions are considered to be a candidate for information carriers in next-generation spintronic devices [119, 179, 180]. A skyrmion can be described

as a nonlinear localised mode with a stable shape. Quantum skyrmions have a history of a few decades [53, 121, 138, 181, 182, 183, 184, 185, 186, 187, 188, 189, 190, 191, 192, 193, 194, 195, 196, 197, 198, 199, 200, 201, 202, 203, 204, 205, 206, 207], whereas magnetic skyrmions have been studied classically with great success since pioneering works [169].

Topological features of a system can impact the robustness of ground-state entanglement properties [208, 209]. Based on this, we investigated the topological entanglement entropy (TEE)—a quantity proposed to be an invariant and a universal quantity of topological phase, in a quantum skyrmion—one of the heavily investigated topological entities in recent literature. Classical skyrmions are topologically stable, meaning they can not be smoothly deformed into a different topological state. Quantum skyrmions, however, lack this strict topological stability. They can, in principle, tunnel to the topologically trivial vacuum state. Despite this, they still possess unique quantum spin properties reminiscent of their classically stable counterparts. TEE has been calculated in toric code systems [210, 211, 212, 213] and in a honeycomb lattice [214, 215]. TEE was earlier defined as a topological invariant and a universal quantity and [213, 216] it is equal to the logarithm of the total quantum dimension of the anyons. Recent investigations suggest that the TEE is not purely an invariant of the topological phase: there exist exceptions where TEE is only an upper bound to the logarithm of the total quantum dimension [217, 218].

We expect that the entanglement entropy in the ground state should reflect the topological nature as some sort of universal feature [216]. There are no accounts for the quantum skyrmion in this perspective in classifying the skyrmion phase from other helical phases (the helical phase represents the parametric phase associated with the states where neighbouring spins form a spiral or helical patterns. skyrmions are helical as well). We attempted to address this issue in our work.

The quantum states associated with the ferromagnetic phase are devoid of entanglement, while quantum phases with noncollinear spin order (helical or quantum skyrmion phase) have complex entanglement properties. In the theoretical model we studied, we observed a discontinuity in the topological entropy corresponding to skyrmion and helical phases. Adjusting the external magnetic field can drive the system from the helical to the quantum skyrmion phase. In the helical phase, TEE shows enhanced fluctuations and a smooth plateau in the quantum skyrmion phase. This enables us to identify both quantum phases and the border between them.

The main result that we report in this paper is that TEE, along with the scalar chirality, can be used to accurately distinguish various topological phases in a helimagnetic system. Additionally, in a skyrmion system, we show that increasing antiferromagnetic next-nearest neighbour interaction increases the range of magnetic field where skyrmions exist. Increasing the parameter J_2 results in decreasing the correlation length of the system, which in turn helps to improve the invariance of TEE in the skyrmion phase.

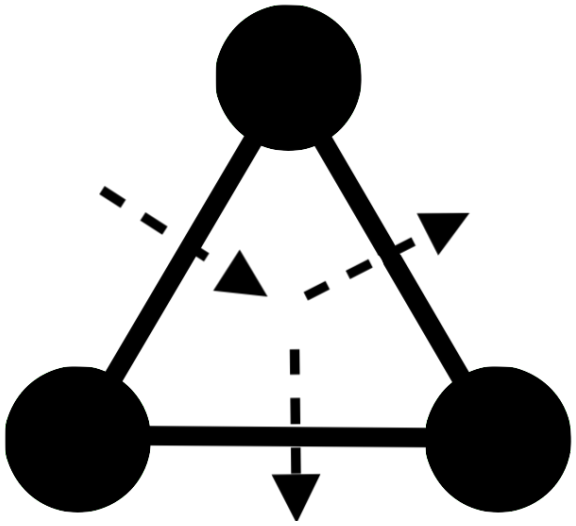

Fig. 3.1 Three bond types(solid lines connecting the dots) and the direction of corresponding DMI vectors(dashed arrows).

3.2 Model and methods

Spin model: We consider a configuration of spins formed in a triangular lattice with periodic boundary condition (PBC) similar to that is considered in Sotnikov *et al.*, 2023 [109]. This configuration possesses a six-fold rotational symmetry and translational symmetry.

The formation of non-collinear magnetic textures like skyrmions is mainly governed by the competing interaction within some spin systems. The competing interactions are either nearest-neighbor ferromagnetic and next-nearest neighbor antiferromagnetic interactions or nearest-neighbor ferromagnetic and the DMI [121, 122, 123, 124, 125, 126, 127, 128, 129, 130, 131, 132, 133, 134, 135, 136, 137]. We consider that the Hamiltonian of the spin-$\frac{1}{2}$ system has the form:

$$\hat{H} = B\sum_i \hat{S}_i^z + J_1 \sum_{\langle i,j\rangle} \hat{\vec{S}}_i \hat{\vec{S}}_j + \quad J_2 \sum_{\langle\langle i,j\rangle\rangle} \hat{\vec{S}}_i \hat{\vec{S}}_j + \sum_{ij} \mathbf{D}_{i,j} \left[\hat{\vec{S}}_i \times \hat{\vec{S}}_j\right], \tag{3.1}$$

Here, competing J_1 (ferromagnetic nearest-neighbour exchange) and J_2 (antiferromagnetic next-nearest neighbour exchange) interactions along with the Dzyaloshinskii-Moriya interaction (DMI) aid the formation of non-collinear magnetic textures. Single angle brackets denote summation over unique pairs of nearest neighbours, and double angle brackets denote summation over unique next-nearest neighbouring pairs. B is an external magnetic field, and the DM vector $\mathbf{D_{i,j}}$ is aligned perpendicular to the bond between lattice sites i and j (see the fig. 3.1). *i.e,* $\mathbf{D}_{i,j} = D\hat{e}_z \times (\mathbf{r}_j - \mathbf{r}_i)$ where $D = |\mathbf{D_{i,j}}|$. We note that in the helical multiferroic insulators, the constant D can be expressed in terms of the magneto-electric coupling g_{ME} with an external electric field E, *i.e.*, $D = g_{ME}E$. Thus, one can control the strength of the DMI term externally [143, 219]. By adjusting the intensity of a high-frequency laser, the DMI interaction can be enhanced. This method involves dynamic control of the intrinsic magnetic interactions through the electronic tunnelling processes

in specific fields. Ultimately, this method leads to the effective re-scaling of DMI and exchange constants in the desired way [151, 152]. The above model with the Hamiltonian as in eq. (B.1) yields peculiar phases in the parameter space. This setting creates the same environment around each spin. Because of this, the physical observables measured on a single spin will give the same outcome for all 19 spins. The DMI term compels the spins to lie in the plane while making a rotation in the local magnetic texture, while the J_1 and J_2 terms encourage the parallel orientation between spins perpendicular to the plane. We noticed that the lower energy levels of the system show variation in degeneracy through various phases. In the supplemental materials [220] fig. B.1, we have shown how degeneracy Γ varies in different phases. The expectation values that we calculate are averaged over these degenerate states. For interested readers, in the supplementary material, we have included the results in the multiplet of degenerate states as well. This paper is based on the following quantities and their implications in the model.

Methods: The formation of a quantum nontrivial magnetic structure can be investigated using spin correlation functions. In particular, we explore the Fourier transform of a longitudinal spin correlation function $G_{\parallel}(\mathbf{q}) = \frac{1}{N}\sum_{ij} G_{\parallel}(\mathbf{r}_{ij})\exp(-i\mathbf{q}\mathbf{r}_{ij})$, where N is the number of spins and the correlation function reads:

$$G_{\parallel}(\mathbf{r}_{ij}) = \langle n|\hat{S}_i^z\hat{S}_j^z|n\rangle. \tag{3.2}$$

Here, n denotes the ground state vector. We expect to see intensity peaks or the Braggs spots in $G_{\parallel}(\mathbf{q})$ for nonzero $\mathbf{q}$ values as a result of the existence of nontrivial magnetic textures [142].

Next, we look at the quantum scalar chirality(C_ψ) used by Sotnikov *et al.* [109] to distinguish between a quantum skyrmion (topological) phase and other phases of the system. C_ψ coincides with the topological invariant, which keeps track of the winding of the magnetization in real space. The classical counterpart of scalar spin chirality is known

for its relation to the topological invariance of classical magnetic skyrmions. For a spin-$\frac{1}{2}$ system the quantum scalar spin chirality,

$$\mathbf{C}_\Psi = \frac{L}{\pi}\left\langle \hat{\vec{S}}_1 \left[\hat{\vec{S}}_2 \times \hat{\vec{S}}_3\right]\right\rangle. \tag{3.3}$$

Here, L is the number of non-overlapping elementary triangular patches covering the lattice and three adjacent spins, S_i where $i = 1,2,3$, forms a patch. The scalar chirality for any of the three adjacent spin combinations represented by spin operators, $\hat{\vec{S}}_i$, acting at the corresponding site, is the same. This is because of the translational and rotational symmetries of the lattice. Scalar chirality indicates the stability of the corresponding skyrmion phase against perturbations as well.

Our main goal is to look for a correlation between the system's topological invariance and entropy. The entanglement entropy (EE) of a system is the measure of the degree of entanglement between two of its composite subsystems. Here we will divide our system into subsystems Q and its complement, $\tilde{Q}$. The composite Hilbert space H_S of the system is a tensor product of the local Hilbert spaces H_Q and $H_{\tilde{Q}}$. Then, the entanglement entropy is calculated by considering the reduced density matrix of the subsystem Q, ρ_Q, and calculating the von Neumann entropy.

$$\mathscr{S}_Q = -tr(\rho_Q \log(\rho_Q)) \tag{3.4}$$

A nonzero value of $\mathscr{S}_Q$ tells us that the two subsystems are entangled. There are quantities that are derived from EE that encapsulate the essence of the topological nature of the system, like TEE.

The bipartite entanglement entropy, or the EE, measures the extent to which one partition of a system is entangled with the next one of the two partitions. It has been found that the EE obeys an 'area law', *i.e.,* the entanglement entropy is proportional to the area of partition boundary [221]. Kitaev and Preskill [216] and Levin and Wen [213] in their

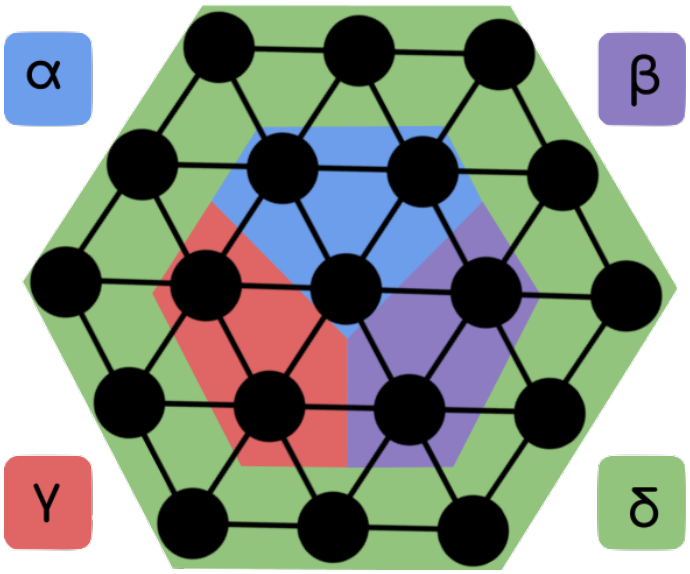

Fig. 3.2 Partitioning of the system for calculating the TEE. Different colours identify corresponding subsystems α, β, γ, and δ.

independent works showed that apart from the area-dependent term there is a part of the entanglement entropy which is universal and characterise a global feature of entanglement in the ground state. This term is coined as the TEE.

Consider the bipartite entropy $\mathscr{S}_Q$ in eq. 3.4 , it has the following form,

$$\mathscr{S}_Q = area(Q)\varepsilon - \zeta + \cdots \tag{3.5}$$

The first term on the L.H.S is dependent on the spacial area, $area(Q)$, of the partition boundary. The second term, $-\zeta$, is a universal additive constant characterising the entanglement in the ground state (TEE). The ellipsis term vanishes with increasing area(Q). In the upcoming paragraph, we will introduce a protocol that can be used to eliminate the boundary-dependent terms and obtain $-\zeta$ or TEE. This brief review on TEE is adapted from Kitaev and Preskill[216].

Consider partitions of the plane of the system α, β, γ, and δ (see fig. C.2). $\mathscr{S}_\alpha$ is the EE of the reduced density matrix ρ_α of the subsystem α, $\mathscr{S}_{\alpha\cup\beta}$ is the EE of the subsystem $\alpha\cup\beta$ with a reduced density matrix $\rho_{\alpha\cup\beta}$ etc. Here, $\cup$ denotes the set operation union.

Then, TEE, $\mathscr{S}_{topo}$ can be obtained using an appropriate linear combination of entropies of the partitions and eq. 3.5 as,

$$\mathscr{S}_{topo} = \mathscr{S}_{\alpha} + \mathscr{S}_{\beta} + \mathscr{S}_{\gamma} - \mathscr{S}_{\alpha\cup\beta} - \mathscr{S}_{\beta\cup\gamma} - \mathscr{S}_{\alpha\cup\gamma} + \mathscr{S}_{\alpha\cup\beta\cup\gamma}. \tag{3.6}$$

Consider the partition α; its boundary is composed of 3 components, the double intersection (boundary) between α and β, α and γ, and α and δ. The boundary term between the partitions α and δ appears once each in $\mathscr{S}_{\alpha}$ and $\mathscr{S}_{\alpha\cup\beta\cup\gamma}$ with a $+$ sign and once each in $\alpha\cup\gamma$ and $\alpha\cup\beta$ with a $-$ sign. Boundary term between α and β appears once each in $\mathscr{S}_{\alpha}$ and $\mathscr{S}_{\beta}$ with a $+$ sign, and in $\mathscr{S}_{\alpha\cup\gamma}$ and $\mathscr{S}_{\beta\cup\gamma}$ with a $-$ sign. Similarly, the boundary term between α and γ appears once each in $\mathscr{S}_{\alpha}$ and $\mathscr{S}_{\gamma}$ with a $+$ sign, and in $\mathscr{S}_{\alpha\cup\beta}$ and $\mathscr{S}_{\gamma\cup\beta}$ with a $-$ sign. We see that all of the three boundary components of the partition α get cancelled in eq. 3.6. In a similar fashion, we can see that boundary-dependent terms of all of the partitions vanish in eq. 3.6. The boundary-independent term $-\zeta$ appears four times with a $+$ sign and three times with a $-$ sign corresponding to the respective entropy terms in eq. 3.6, this leaves only $-\zeta$. For a system with large partition boundaries compared to the correlation length, $\mathscr{S}_{topo}$ is defined to be invariant under smooth deformations of the Hamiltonian and will only vary when the system encounters a quantum critical point. More details on the numerical methods and computing resources used are provided in the supplementary material section titled "Supplementary methodsB-II."

3.3 Results and discussion

We employed a systematic approach to characterise the system into various phases, like the quantum skyrmion phase. First, we consider the Fourier transform of the longitudinal spin correlation function known as the structure factor. The structure factor of the helical ground

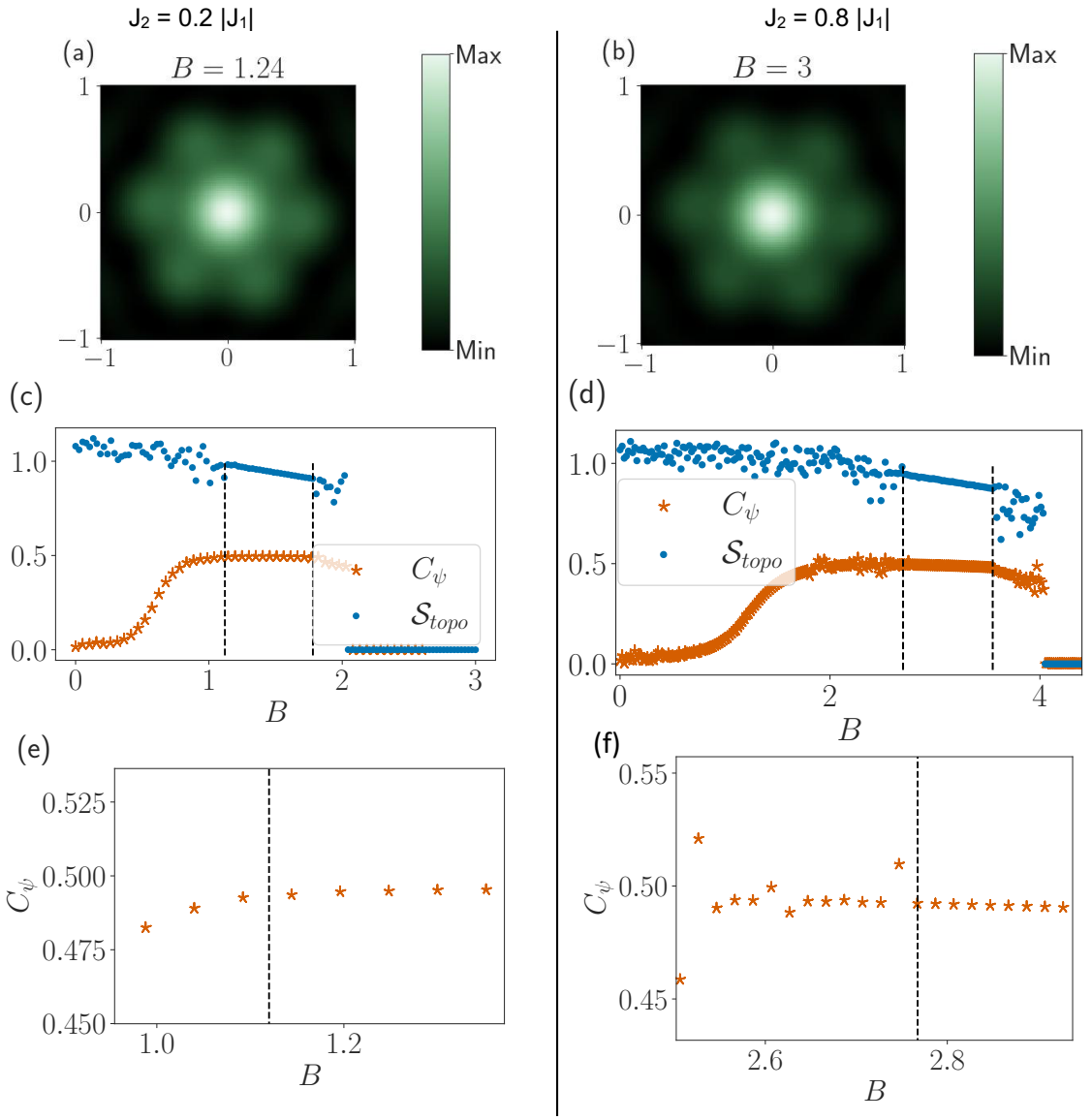

Fig. 3.3 (a-b) Fourier transform of the longitudinal structure factor calculated for (a) $J_2 = 0.2|J_1|$, $B = 1.24|J_1|$ and (b) $J_2 = 0.8|J_1|$, $B = 3.0|J_1|$. (c-d) TEE and $\mathbf{C}_\psi$ vs applied field for (c) $J_2 = 0.2|J_1|$ and (d) $J_2 = 0.8|J_1|$. (e-f) Chirality zoomed for $J_2 = 0.2|J_1|$ and (f) $J_2 = 0.8|J_1|$. For all the graphs, $D = 2|J_1|$, $J_1 = -1$.

state exhibits six peaks, reflecting the inherent 6-fold rotational symmetry of the system (See also Fig. B.1 and Fig. B.3 from the supplementary file). However, in the skyrmion state, this symmetry is spontaneously broken, manifested by the emergence of a single dominant peak at $\mathbf{q} = 0$, accompanied by the suppression of the six peaks at $\mathbf{q} \neq 0$. In the

helical phase, the peaks are not sharply defined at specific reciprocal lattice points, instead appear diffused and overlapping. Conversely, the skyrmion and ferromagnetic phases exhibit a well-defined peak only at $\mathbf{q} = 0$. This observation suggests that translational symmetry is broken in the helical phase but is restored in the skyrmion and ferromagnetic phases.

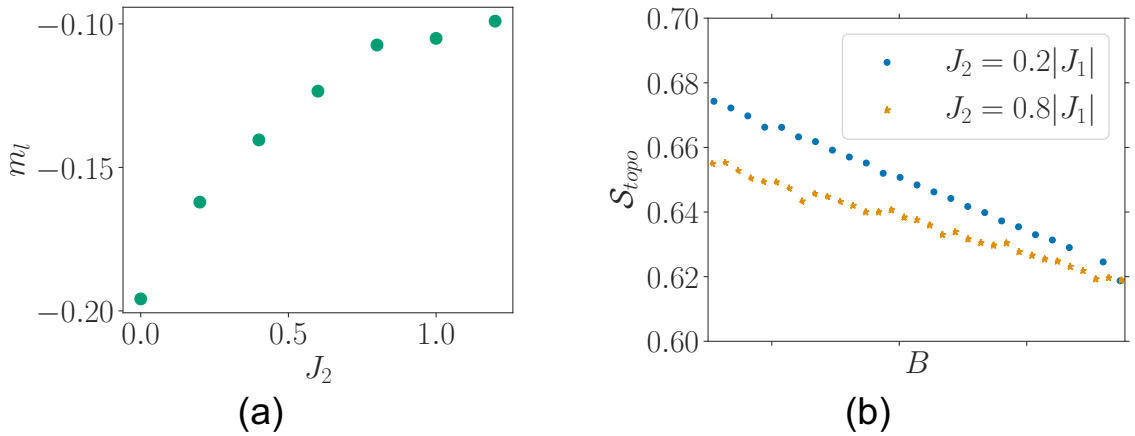

Fig. 3.4 (a) The linear part of TEE is plotted for two different J_2s. This shows that for larger J_2, the slope is less. Note that in this plot, the axes do not signify absolute values of the quantities; the purpose is to compare the slopes only. (b) The slope of the linear part of TEE, m_l vs the parameter J_2. $D = 2|J_1|$, $J_1 = -1$ are used for all of the graphs.

The Fourier transform of the longitudinal spin correlation function reveals distinct spin textures for two parameter sets (Figs. 3.3(a) and 3.3(b)) contrasting sharply with the helical phase. Faint Bragg peaks at nonzero $\mathbf{q}$, alongside a prominent peak at $\mathbf{q} = 0$ indicate spin configurations distinct from the helical. Overlapping peaks at nonzero $\mathbf{q}$ in the structure factor (Supplementary material Fig. B.3) are the hallmark of a helical phase. In contrast, a dominant peak at $\mathbf{q} = 0$ with significantly diminished peaks at nonzero $\mathbf{q}$ signals a skyrmion phase, distinct from the helical order. while a sole peak at $\mathbf{q} = 0$ characterizes the ferromagnetic phase. The quantum scalar chirality, which is the quantum variant of classical chirality—generally used to characterise skyrmions [109], shows three phases of the ground state. We can clearly distinguish between a helical phase and a trivial ferromagnetic phase (see fig. 3.3: (c,d) orange curves are the scalar chirality (C_ψ),

and its zero corresponds to the trivial phase). Here, the transition from the helical to the skyrmion phase is slow (continuous and fluctuation-free and not distinguishable), and we do not observe a boundary between them. We use eq. (4.4) and compare it with the TEE to determine the boundary between various phases.

Following the literature [109], the plateau of C_ψ can be associated with a skyrmion phase. However, C_ψ fails to show a transition from the helical phase to the skyrmion phase, where it exactly becomes flat or parallel to the x-axis (see fig. 3.3 (c,d) orange curves). For instance, in fig. 3.3 (c), at the applied field $B \sim 1.0|J_1|$, the chirality seems to achieve a plateau. But in reality, the value is still varying slowly (zoomed-in fig. 3.3 (e)). Although the chirality demonstrates the robustness of a given skyrmion phase, it fails to show a clear boundary between different phases. Therefore, relying only on C_ψ to determine the topological phases in a skyrmion system may lead to errors because it is difficult to pinpoint where the helical phase ends and where the skyrmionic phase begins. By contrast, the TEE (in blue) shown along with C_ψ in fig. 3.3 (c) is characterised by a continuous and fluctuation-free curve, which is associated with a topologically protected phase of the skyrmion. Thus, TEE, along with C_Ψ precisely identifies the three phases: (i) the TEE is zero for the trivial phase; (ii) it is scattered for a helical phase; and (iii) it is continuous for a skyrmion phase. In fig. 3.3 (d), we have TEE and C_ψ plotted for a different J_2 ($0.8|J_1|$) value. Here, we see that, for larger next-nearest antiferromagnetic interaction, the topological phase remains robust against a stronger applied magnetic field. TEE helps to identify a transition from a helical to a skyrmionic phase as well. Figures showing a zoomed view of the phase boundaries (vertical dashed lines) established by TEE are provided in the supplementary file fig. B.6. The slow variation of the scalar chirality before crossing this critical boundary is visible in fig. 3.3 (e), and the constant plateau achieved by the chirality can be seen after the critical point in fig. 3.3 (f). Now, with these newly established boundaries, we can see that the states represented by fig. 3.3 (a-b) are

in the skyrmion phase. Here, the ground state is non-degenerate, unlike the helical phase, which has a six-fold degeneracy in the ground state. The structure factor for the six-fold helical multiplets of states is shown in supplementary material fig. B.3.

We verified the universality of the fluctuating TEE in the helical phase by studying TEE in different system sizes of the same Hamiltonian eq. B.1. The results are shown in the supplementary file fig. B.9. The fluctuation does not vanish/decrease with the increasing system size, implying that the fluctuation is not an artefact of finite size but is universal. The schematics for the spin lattices with $N = 7$ and $N = 13$ are provided in the supplementary file fig. B.10. The geometry of the $N = 19$ lattice is the same as the lattice shown in the schematic, fig. C.2.

For a two-dimensional system having a topologically protected phase, the TEE would show a constant plateau around the corresponding applied field if the system boundary is large enough compared to the correlation length. Due to the finite size limit, this is not realisable in this system. Because of computational limitations, making a scaling analysis is currently difficult. We note that classical skyrmions are studied in numerical micromagnetic calculations. Typically, classical skyrmion consists of more than a hundred magnetic moments. For example, in a recent paper [143], roughly 200 classical magnetic moments were employed. At the current stage, we cannot reach this number of spins in quantum calculations using the exact diagonalisation method. However, we see that already adding the next ring to the $N = 19$ spin quantum skyrmion destroys it. Conversely, one cannot shrink the classical skyrmion below a certain number of magnetic moments without destroying it. The lower limit of the number of classical magnetic moments in the classical skyrmion is far higher than the scale of quantum skyrmions. Thus, the capacity of quantum calculations is not the main problem in the realisation of classical to quantum transition. Quantum and classical skyrmions are quantum and classical topological solitons, respectively, but they have different natures. The criteria to obtain a classical skyrmion

is a topological charge, and the topological charge is not valid for quantum skyrmions. Quantum skyrmions are characterised by scalar chirality. However, in our paper, we showed that TEE, along with scalar chirality, more precisely characterises the topology rather than scalar chirality alone since scalar chirality does not distinguish two topological phases: quantum skyrmion phase and helical phase. Conversely, TEE behaves differently in those two phases: In the helical phase, TEE fluctuates strongly, meaning that TEE is not a good quantum number in the helical phase, and in the quantum skyrmion phase, TEE is a stable quantum number. To summarise the response to this question: When shrinking to a smaller size, classical skyrmion gets destroyed before reaching the quantum limit, and quantum skyrmion, upon extension gets destroyed before reaching the classical skyrmion limit. Therefore, we cannot observe a smooth transition from the quantum to the classical skyrmion limit even if we hypothetically assume that it is possible to exactly diagonalise the 200-300 spin system. Nevertheless, if we compare the slopes, $m_l = \frac{\Delta(\mathscr{S}_{topo})}{\Delta(B)}$, of the linear part of the TEE, for two different values of J_2, we can see that the TEE has a lesser slope for larger J_2 value than that for smaller J_2 value. This is shown in fig. 3.4(a). For $J_2 = 0.2$ and $J_2 = 0.8$, the linear parts of the TEE make angles ~ -0.2 radians and ~ -0.1 radians, respectively, with respect to the positive x-axis. This comparison is demonstrated in fig. 3.4(a). We can clearly see that a larger J_2 results in a smaller slope. In fig. 3.4(b), we have plotted the slope of the linear part of TEE vs the parameter J_2. We see that the slope of the linear part of the TEE moves closer to zero as we increase J_2. This tells us that the linear part is approaching a constant plateau as we increase J_2; this is owing to the increased frustration introduced with a larger J_2 value enhancing the formation of the non-collinearity. Or, maybe because the increase of J_2 induces a bulk effect, just as if the system size is increased. In supplementary materials, fig. B.7, and the discussion therein, we have shown that the correlation length of the system decreases with increasing J_2.

3.4 Conclusions

Compared with the ferromagnetic state, quantum states with noncolinear magnetic order are not product states, and they are therefore characterised by nontrivial entanglement properties. Besides, quantum states with noncolinear magnetic order can be diverse. Paradigmatic examples are helical and quantum skyrmion phases. The helical phase is not topologically protected, or we do not find an invariant of the control parameter, whereas the scalar spin chirality and topological entanglement entropy topologically protect the quantum skyrmion phase. What is important is that in the quantum case, as opposed to the classical case, it is rather demanding to distinguish between these two phases. The reason is that the standard argument about classical magnetic textures does not apply to the quantum case. Consequently, one needs to find other criteria that are valid for the quantum case. Identifying the quantum phase transition between two helical and quantum skyrmion phases is an even more complicated problem. In this work, we explored one of the crucial properties of a quantum many-body system, entanglement entropy, in the context of the topological protection of a quantum skyrmion system. We used entropic measures of entanglement to classify the skyrmion phase uniquely. We investigated two quantities: quantum scalar chirality and topological entanglement entropy. We used these two quantities to identify topological ordering in quantum many-body systems. Scalar chirality was exploited for quantum skyrmions in the past. However, up to our knowledge, topological entanglement entropy has never been discussed in this context before. Though the scalar chirality succeeds in comparing the robustness of two skyrmion phases, it fails to establish a clear boundary between the helical and the skyrmionic phases. In the present work, we discovered that unlike the scalar chirality and the topological index, the topological entanglement entropy precisely distinguishes between helical and quantum skyrmion phases and infers quantum phase transition between those two phases. Adjusting the external magnetic field can drive the system from the helical to the quantum

skyrmion phase. We found that topological entanglement entropy behaves differently in each quantum phase. In the helical phase, TEE shows enhanced fluctuations and a smooth plateau in the quantum skyrmion phase. The universality of fluctuating TEE in the helical phase and zero TEE in the ferromagnetic phase are evident from our observations. Thus, we cannot overlook the potential universality of the unique behaviour exhibited by TEE in the skyrmion phase. Even without a universality clause in the skyrmion phase, the universal behaviour exhibited by the system in the other two contexts is sufficient to determine the phase boundaries as long as a plateau exists in the associated scalar chirality. Finally, based on the topological entanglement entropy, we provide a numerical proof for the observation that the quantum skyrmion model we discussed shows robust topological properties when we increase the next-nearest exchange coupling J_2 within the skyrmionic phase.